Corrosion Science 51 (2009) 1519–1527

Contents lists available at ScienceDirect

Corrosion Science

journal homepage: www.elsevier.com/locate/corsci

A combinatorial passivation study of Ta–Ti alloys

Andrei Ionut Mardare [a,b], Alan Savan [b], Alfred Ludwig [b], Andreas Dirk Wieck [b], Achim Walter Hassel [a,*]

[a] Max-Planck-Institut für Eisenforschung GmbH, Max-Planck-Str. 1, 40237 Düsseldorf, Germany
[b] Ruhr-Universität Bochum, 44780 Bochum, Germany

ARTICLE INFO

Available online 13 December 2008

Keywords:
A. Tantalum, titanium
B. Combinatorial electrochemistry, scanning droplet cell
C. Anodic films

ABSTRACT

A combinatorial study of the kinetics of anodic oxide formation was performed on a co-deposited Ta–Ti composition spread sample (from 2 to 76 at.% Ti). The samples were characterized by High Resolution Scanning Electron Microscopy (HRSEM) and Grazing Angle X-Ray Diffraction (GIXRD). High-throughput-screening was performed with an automated scanning-droplet-cell to anodise incrementally by cyclic voltammetry and perform electrochemical impedance spectroscopy. A comprehensive set of oxide parameters, including film formation factor, dielectric constant, specific oxide resistance, flat band potential and donor density was obtained. The observed changes could be directly correlated to the microstructure of the parent metal.

1. Introduction

Ta has puzzled scientists since its discovery in 1802. Its inertness against the strongest agents, including aqua regia, misdirected scientists trying to determine its standard electrode potential, leading them to conclude that Ta was a noble metal. Its unusual behaviour is directly seen in its remarkably simple Pourbaix diagram. Ti was also discovered first in its oxide form [1] .

Important applications of both metals come from the fact that they show a remarkably effective passivation [2] and they are referred to as valve metals. Today, Ta is predominantly used for capacitors in which the higher relative permittivity number of the oxide as compared to Al justifies the higher price of the metal. Ti is used as a biomaterial, in the aviation industry, for chemical reactors and for other applications in which a light metal with good mechanical properties and high chemical stability is needed. The similarity of the two metals Ta and Ti, together with some interesting differences in the metal and metal oxide properties suggest a thorough investigation of their binary alloys.

Ta is body centred cubic (bcc) and Ti hexagonal close packed (hcp). Alloying Ti with Ta can stabilise the high temperature modification β-Ti in which it is also bcc. The two separating boundaries $\alpha/(\alpha+\beta)$ and $\beta/(\alpha+\beta)$ are pointing to an intersection at 4 at.% Ta and approximately 38 at.% Ta [3]. It is worth mentioning that addition of Ta selectively extends the *c*-axis of the hexagonal α-Ti while leaving the *a*-axis unaffected.

Zhou et al. have studied the mechanical properties of Ta–Ti alloys in 10% compositional steps for biomedical applications. Some of them show an interesting combination of high strength and low modulus [4]. This study was later extended to a comparison between Ta and Hf for alloying with Ti. Earlier, Chen and Liu studied the formation of metastable alloys created by ion mixing through irradiation of multilayered samples. They constructed Gibbs free energy diagrams to explain the unusual alloying behaviour [5].

Ruth and Schwartz investigated the composition of oxide films formed anodically on Ta–Ti thin films by means of Rutherford backscattering. They found a film formation factor of 1.88 nm V^{-1} for a nearly equiatomic parent metal composition. Amorphous uniform mixtures of Ta_2O_5 and TiO_2 were formed, covered by a thin layer of pure TiO_2, about 3% of the mixed oxide's thickness [6].

The gas phase oxidation kinetics of Ta–Ti alloys were investigated in the temperature range from 800 to 1400 °C by Hanrahan and Butt. The situation is quite complex here, since oxygen acts as α-phase stabilizer while Ta stabilises the β-phase of Ti. Ta decreases the diffusivity of Ti and the solubility of oxygen. As a result the relation between composition and minimum oxidation rate depends on the temperature and the atmosphere [7]. Even in the Ni–Ti system it was found that Ti moves faster leading to an enrichment of TiO_2 in the outermost layer. For this system, it is easier to explain since there are significant differences in oxygen affinity between both metals which is not the case for the Ta–Ti system [8].

de Souza and Robin performed corrosion studies of four different Ta–Ti alloys in sulfuric acid [9]. They saw the main advantage in an increase of the corrosion resistance of Ti against reducing acids by alloying it with Ta, for applications in which the cost of pure Ta is prohibitive. A similar result was obtained by Zhou et al., who looked at the corrosion resistance of Ta–Ti alloys for biomedical applications and suggested higher Ta contents for improved corrosion resistance [10].

The most comprehensive work in studying the properties of anodic films on Ta–Ti was carried out by Mato et al. [11]. This study

* Corresponding author. Tel.: +49 211 6792 464; fax: +49 211 6792 218.
E-mail address: hassel@elchem.de (A.W. Hassel).

0010-938X/$ - see front matter © 2008 Elsevier Ltd. All rights reserved.
doi:10.1016/j.corsci.2008.12.003

was conducted on sputter-deposited Ta–Ti alloys in the range from 0.6 to 40 at.% Ti. They confirmed the formation of a thin TiO_2 layer on the mixed TiO_2 and Ta_2O_5 film. The film formation factors varied in the range from 1.6 to 1.9 nm V^{-1}. It is noteworthy that the same film formation factor was found for all alloys with a Ti content of up to 17 at.%, except for the Ta-40 at.% Ti alloy. The relative permittivity number of the oxides formed was essentially constant in the range between 27 and 30.

Nowadays, alloying of Ta with Ti for an increase of the oxide's permittivity is under investigation. A significant increase of the oxide permittivity is found only at higher Ti contents, at which the breakdown stability of the oxides decreases significantly.

So far all experiments were performed on discrete alloys of uniform composition. This limits the number of investigated compositions since each sample has to be prepared individually. This is a significant effort, taking into account the high melting points of the pure metals and their extreme oxygen affinity, requiring sophisticated metallurgical equipment. Recently, a novel approach was chosen to perform a high throughput investigation of the passivation behaviour of a binary composition spread sample [12]. Such a sample can easily represent 100 or more compositions, depending on the concentration gradient and the spatial resolution of the local investigation method. Combining this approach with a fully automatic scanning droplet cell [13–14] enables an efficient, systematic (high throughput) scanning of such a system. In the Al–Fe system investigated before, an unexpected singularity of the oxide properties was found around 12 at.% Fe, demonstrating the advantage of this approach. A closer look into the system was taken and the observed behaviour was assigned to reaching the percolation threshold of dopant atoms.

In this work, a similar approach is made to study the passivation behaviour of Ta–Ti alloys in the range from Ta-2 to Ta-76 at.% Ti.

2. Experimental

2.1. Preparation of Ta–Ti composition spread library

Ta–Ti gradient composition samples were fabricated using a co-sputtering technique in an ultra-high vacuum system (DCA, Finland) using two sputtering targets, 101.6 mm in diameter, that were aimed target center to substrate center and placed at an angle of 144° one to another. Ta was sputtered from a high purity target (99.995%, Kaistar R&D) using a power of 200 W RF, leading to a sputter rate of 0.73 nm s^{-1}. Ti was sputtered from a target with 99.995% purity (Williams Advanced Materials) using a power of 200 W DC. Three thermally oxidized Si wafers with a diameter of 100 mm were sequentially used as substrates for the co-sputtering depositions in order to obtain a Ta–Ti library with a total compositional spread ranging from 2 to 76 at.% Ti. For all samples, the base pressure of the chamber was in the range of 2×10^{-6} Pa. The depositions were carried out at room temperature in Ar atmosphere with a pressure of 6.66×10^{-1} Pa. The target-substrate distances were approximately 19 cm, leading to the formation of wedge-shaped thin films of each metal with a total thickness of about 300 nm at the wafer center.

Additionally, pure Ti and pure Ta reference thin films were deposited using single target sputtering in the same vacuum chamber and with the same deposition parameters. After the deposition of the composition spread libraries, energy dispersive X-ray spectroscopy (EDX) was used for the mapping of the chemical composition of the sample surface.

2.2. Scanning droplet cell

A three-electrode configuration, capillary-based microelectrochemical cell, known in the literature as the scanning droplet cell (SDC), was used for the local anodization of the Ta–Ti alloys [13]. A 2.5 mm diameter borosilicate capillary was pulled using a puller (PC-10, Narishige) for serving as the outer body of the cell and a tip with a diameter of 200 μm was obtained using a micro-grinder (EG-400, Narishige). The reference electrode of the cell was a capillary μ-AuHg/$Hg_2(CH_3COO)_2$/$NaCH_3COO$ reference electrode having an 1 mm outer diameter and a 100 μm tip diameter. An Au stripe (1 mm wide) was used as counter electrode, wrapped around the reference electrode capillary and together with the reference electrode into the main was inserted body capillary. All components of the SDC were mounted into a plastic block as previously reported [14,15]. A silicone gasket was fabricated at the tip of the cell by immersing it into liquid silicone followed by drying in nitrogen flow. For ensuring a reproducibly wetted surface (working electrode) on the Ta–Ti alloys, the tip of the cell was pressed against the investigated surface. In this way, the electrolyte–air contact was prevented and the volume expansion of the electrolyte droplet due to electrocapillarity during the measurements was avoided [16].

2.3. Hardware description and measurements details

For dosing the electrolyte from the cell, a computer controlled micro-syringe pump (Micro 4, World Precision Instruments) combined with a 100 μl syringe was used. The electrical contact to the thin film parent metal surface was achieved using a W needle pressed against the sample. Due to the compositional spread along the surface of the samples an automated high throughput approach was used. The tip of the SDC was moved across the sample surface by a computer controlled 3D scanner actuating XYZ translation stages. Using a LabView control and a self-developed data acquisition software, automation of the high throughput experimentation was achieved. Details about the software can be found elsewhere [14]. A force sensor (KD45 2N, ME-Messsysteme) combined with a lock-in amplifier (EG&G 7265) was used for the automated control of the applied force for pressing the tip of the SDC in a highly reproducible way, at a defined value of 3 mN against the sample. The measured error in the diameter of the wetted spots on the surface of the alloys was smaller than 1% as it was confirmed on a Hf sample [17]. The microstructure of selected samples from the composition spread was characterized by SEM and 1° grazing incidence X-ray diffraction (GIXRD) at different concentrations. The X-ray spot, approximately 3 mm wide, had a suitable size for such investigations, since the EDX mapping revealed a compositional gradient of 0.25 at.% mm^{-1}. The surface was locally anodized in an acetate buffer electrolyte (pH 6.0) prepared from reagent grade chemicals and de-ionized water using a potentiostat (EG&G Pstat/Gstat 283, AMETEK Princeton Applied Research). In this work, all the potentials are given with reference to the standard hydrogen electrode. The surface of the Ta–Ti composition spread was scanned with a resolution of 1 at.% and small oxide spots were locally grown. The anodizations were carried out potentio-dynamically at a potential scan rate of 100 mV s^{-1}. Cyclic voltammograms having the upper potential limit between 1 and 10 V were sequentially recorded in 1 V steps for each investigated region. Before each cyclic voltammogram, the impedance of the already-formed oxide layer was measured at high (1 kHz) and low (0.1 Hz) frequency using a frequency response analyzer (S5720C, NF Electronic Instruments) with a 10 mV AC voltage perturbation in order to measure the dielectric constant and electric resistivity of the anodic oxides in between their stepwise growth. For various concentrations of the parent metals, Mott–Schottky analysis was conducted by measuring the capacitance of a 3 V potentio statically grown anodic oxide for different DC biases. X-ray photoelectron spectroscopy (XPS) was used for the in-depth qualitative evaluation of the Ta–Ti library at different compositions. The anodic oxides were probed at different depths using Ar sputtering with a sputter rate of 0.1 nm s^{-1}.

3. Results and discussion

3.1. Ta–Ti binary library microstructure

A bulk mixture of Ta and Ti can result in a β stabilized phase for Ta concentrations >83 at.% at 400 °C. The isomorphous type Ta–Ti phase diagram shows a wide immiscibility gap and an α phase for very low Ta contents [18]. However, co-deposition of Ta and Ti at low temperatures can be expected to produce metallic thin films, possibly showing deviations from the bulk phase diagram.

The microstructure of the Ta–Ti alloys was investigated using SEM and in Fig. 1 the surface of the Ta–Ti combinatorial library is presented as a function of the concentration. The microstructures observed on pure Ta and Ti thin films are shown as reference. On the surface of pure Ta thin films, two different types of grains can be observed. The majority round shaped grains have a diameter of about 100 nm and are forming a compact structure. A smaller number of slightly bigger triangular grains can also be observed. The addition of Ti changes the microstructure, leading to the disappearance of the bigger triangular shaped grains. At Ta-5 at.% Ti, the alloy surface shows small grains of around 50 nm clustered along the boundaries of bigger domains. This structure continuously evolves with the increase of Ti content so that at Ta-20 at.% Ti, again a compact structure of round shaped grains is obtained. Between 20 and 30 at.% Ti, the metallic grains start to arrange preferentially on a single direction which has a complicated dependence to the positions of the sputtering targets. Starting at Ta-40 at.% Ti, the presence of domains of oriented grains could be observed up to a composition of Ta-65 at.% Ti, when the grain alignments could not be detected anymore. Increasing the Ti concentration even more, new grains with a pyramidal aspect evolve and their diameter grows from around 100 nm at 70 at.% Ti to almost 400 nm at 80 at.% Ti resembling the structure obtained on the pure Ti thin films.

The surface of pure Ti thin films deposited on silica shows an agglomeration of nanocrystals bigger than 100 nm in diameter with voids in between. The electric conductivity of these nanocrystals combined with the rough surface complicate the interpretation of electrochemical measurements achieved on pure Ti films, the current plateau recorded during the potentiodynamic oxide formation being overestimated due to much lowered current efficiencies. Therefore, in this work the electrical and electrochemical properties of anodic oxides grown on pure Ti will be referenced to the literature [19,20].

Fig. 2 shows the crystallographic orientations of the Ta–Ti thin films as measured by XRD. The intensity scale is logarithmic to simplify comparing the location of the peaks. The diffraction patterns of pure Ta and Ti are also shown. Pure Ta thin films show a tetragonal structure whereas pure Ti thin films are hexagonal. Also, the positions of the peaks corresponding to the cubic phase are shown for both pure metals.

Addition of small amounts of Ti in Ta leads to the disappearance of the diffraction peak on the (5 1 3) plane at Ta-5 at.% Ti, which corresponds to the disappearance of the bigger triangular shaped grains (see Fig. 1). Even though the surface grains are continuously evolving as shown in the SEM images of Fig. 1, the crystallographic orientations do not show significant differences until the grains start aligning at Ta-30 at.% Ti. In the compositional range corresponding to the surface domains formation between Ta-35 and Ta-65 at.% Ti, the presence of the cubic (2 0 0) plane can be observed. From Ta-40 at.% Ti the alloy structure changes to the cubic phase. This β stabilization of the alloys remains constant with the

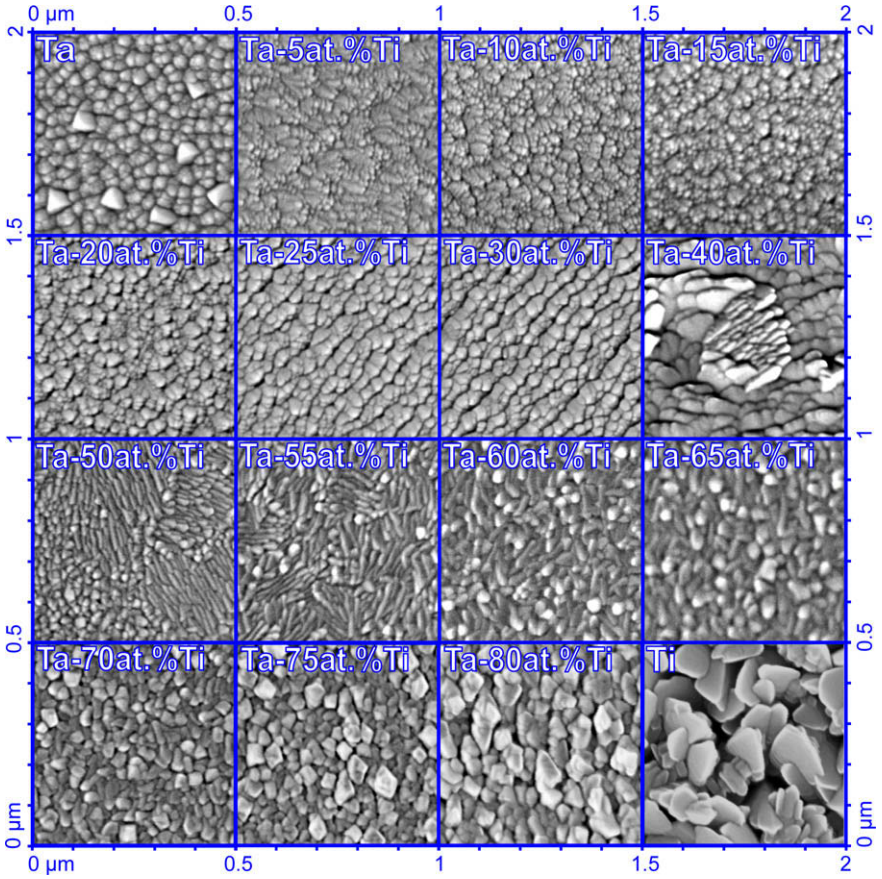

Fig. 1. SEM images of the surface of the Ta–Ti binary composition spread for different concentrations. The surfaces of pure Ti and Ta are presented as references.

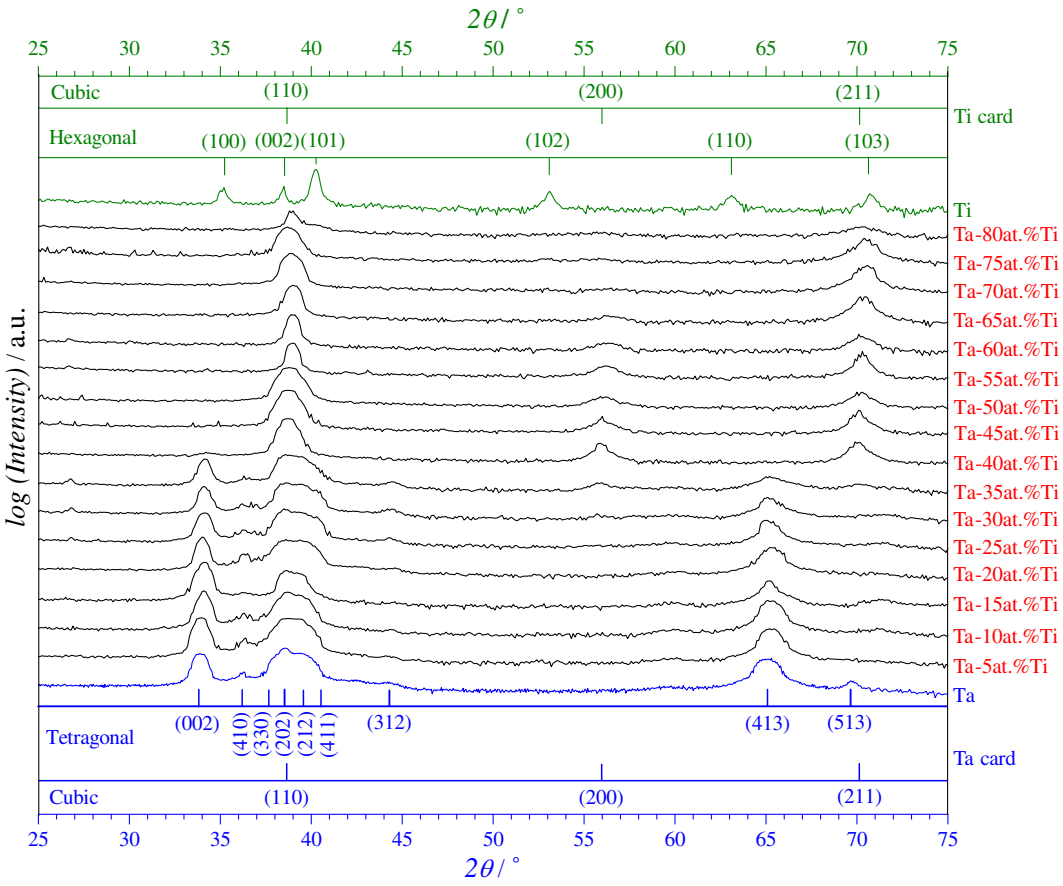

Fig. 2. XRD patterns measured locally for different concentrations on the Ta–Ti composition spread.

increase of Ti and the surface domains dissolution at Ta-65 at.% Ti coincides with the disappearance of the diffraction peak on the (200) plane. The formation of grains at high Ti concentrations still have a cubic structure, with only <110> and <211> orientations clearly visible. No indications of the hexagonal or tetragonal structures could be observed up to 80 at.% Ti in the alloys. The XRD information match closely the grain evolution imaged by SEM and together provide information about the microstructure of the Ta–Ti binary combinatorial library.

3.2. Potentiodynamic oxide formation and characterization

Fig. 3 shows several cyclic voltammogram series recorded during the anodization of Ta–Ti alloys for different concentrations. In each voltammogram corresponding to the step-wise anodizations from 1 to 10 V in an anodization series, a current density plateau was observed. This corresponds to the anodization process dictated by Faraday's charge–mass correlation applied to a potentiodynamic process with a constant rate of potential increase in the absence of side reactions such as oxygen evolution. The value of the current density plateau is directly related to the inverse of the field strength of oxide formation, known as the oxide formation factor k [21], which is given by:

$$k = i_{ox} K_{ox} v^{-1}$$

where i_{ox} is the plateau current density and v is the rate of voltage increase during the potentiodynamic scans. K_{ox} is an oxide constant depending on oxide density, molar mass and number of electrons per formula unit exchanged during the oxidation of pure metals or alloys. The density of the anodic oxide grown on the Ta–Ti alloys

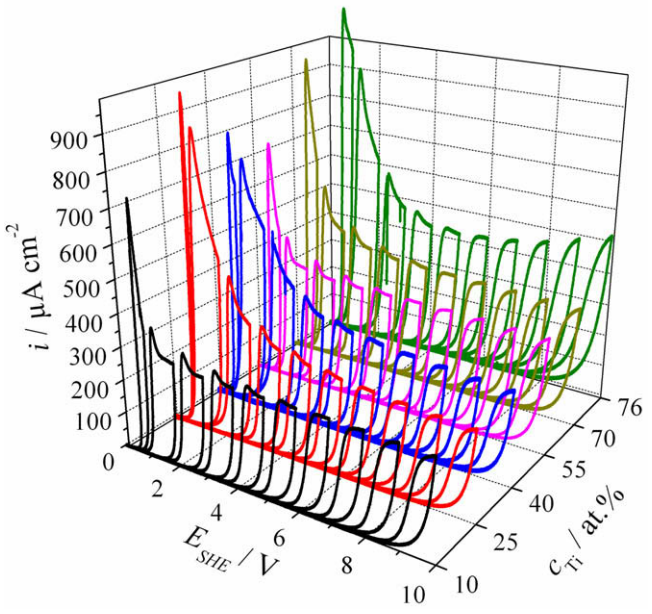

Fig. 3. Cyclic voltammograms recorded during the potentiodynamic oxide growth on Ta–Ti binary alloys for different concentrations.

was calculated using a mixed matter model as a function of the parent metal concentrations by means of a linear distribution between the densities of pure Ta_2O_5 and TiO_2 (8.1 and 4.22 g cm^{-3}, respectively).

At the beginning of each cyclic voltammogram, a sudden current increase was observed, especially at low oxidizing potentials. This overshoot in the current characterizes a delayed oxide formation due to charge accumulation in a space charge layer inside the previously grown oxide [22]. The anions accumulate inside the oxide at the oxide/electrolyte interface while the cations accumulate at the oxide/metal interface. The position of the maximum current peak coincides with the beginning of the overlapping of the two charged regions inside the oxide and the complete overlap will result in the current stabilization plateau and the simultaneous oxide growth at both interfaces. This dynamic is a direct consequence of the high-field regime of the anodic oxide growth [22]. Due to a constant potential scan rate, a weaker field strength increase is achieved for thicker initial oxides and as a result the current overshoots are less visible at higher potentials. At potentials higher than 4 V the retardation of the migrating ion clouds dominates the kinetics of oxide formation. This results not only in a smeared out increase of the oxide formation current but also in a delayed increase, as can be directly seen from the increasing gap between two subsequent oxide formation curves with increasing oxide formation potential.

For all alloys, a valve metal behaviour was observed in the strong current decay at the end of each cyclic voltammogram, when the electric field decreases due to the change of the potential scan direction and the ion hopping activation energy described by the high-field model is no longer achieved.

Full impedance spectra were recorded at different concentrations for determining the general behaviour of the anodic oxides in the Ta–Ti combinatorial library before the automated single frequency impedance measurements. Several impedance spectra measured for a wide frequency range on oxides potentiostatically grown at 3 V, for various concentrations on the metallic library are presented in Fig. 4. The impedance (a) and the phase shift (b) are plotted as a function of frequency for an applied bias of 0 V (SHE). For all concentrations in the Ta–Ti combinatorial library, the impedance showed a typical −1 slope in the double-logarithmic plot. The phase shift rapidly reached values close to −90°, 1 kHz being the highest frequency where the fully shifted phase suggests a pure capacitive behaviour. This shows that the automatic measurements of single frequency impedance at 1 kHz is suitable for capacitive characterization of the anodic oxides along the concentration gradient in the Ta–Ti combinatorial library. The impedance data suggest that a simple RC parallel circuit characterizing the oxide, in series with the electrolyte resistance, can be used for describing the anodic oxide, as is typical for oxides on valve metals such as Ta [22]. The semiconductor behaviour of Ti oxides is not so obvious under these conditions.

The surface of the entire Ta–Ti composition spread was scanned using the SDC and the properties of the anodic oxides were mapped as a function of the metal parent concentrations. The oxide formation factors were directly calculated from the current density plateaus [21]. The dielectric constants of the forming oxides were obtained from the slope of the linear dependence between the inverse capacitance of the oxides and their formation potentials (related to the oxide thicknesses through the oxide formation factors). Similarly, the slopes of the linear dependence between oxide resistances (measured by impedance analysis at low frequency) and their formation potentials, directly yielded the oxide electrical resistivities. Fig. 5 shows the oxide formation factors together with their dielectric constants (a) and the oxide electrical resistivities (b) measured for the entire compositional range of the Ta–Ti composition spread. All curves were fitted using multipeak Lorentzian functions. The properties of the anodic oxides grown on pure Ta and Ti were added as reference.

Starting from a value of 1.8 nm V^{-1} measured on a pure Ta thin film, the oxide formation factors of the Ta–Ti alloys decrease

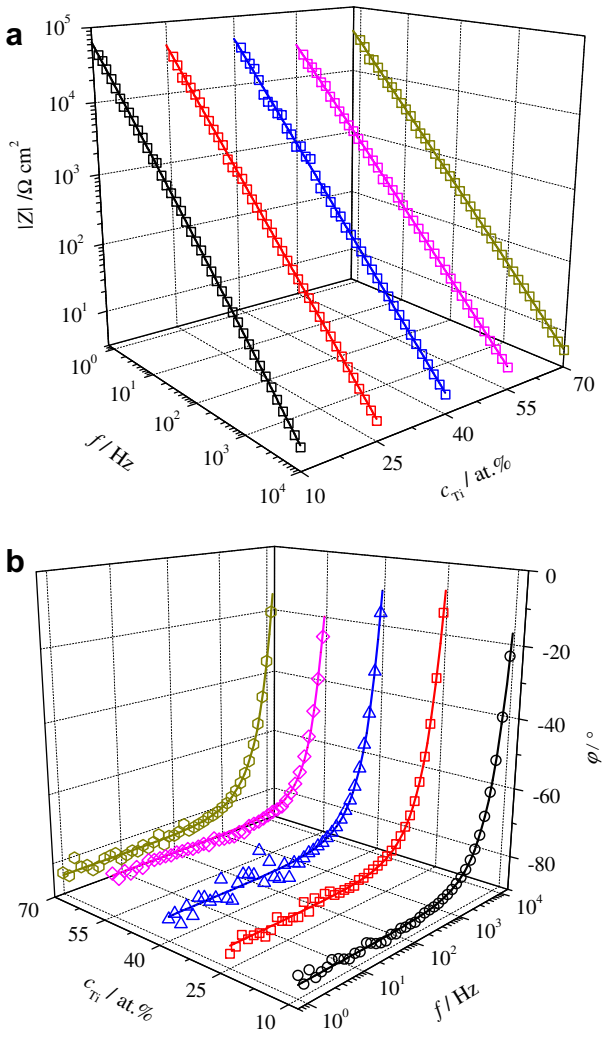

Fig. 4. Electrochemical impedance spectroscopy measurements of the anodic oxides grown potentiostatically at 3 V on the Ta–Ti composition spread for different concentrations.

slightly upon addition of small amounts of Ti. A relatively constant value of 1.7 nm V^{-1} was measured for Ti concentrations of up to 20 at.%. This can be associated with the parent metal grain structure evolution shown in Fig. 1. Up to Ta-20 at.% Ti a compact structure with homogeneous grain sizes was observed. The composition region between 20 and 30 at.% Ti where the metallic grains start to align in Fig. 1, shows a linear increase of the oxide formation factors. This can be attributed to structural changes in the parent metals combined with a linear change in the surface roughness due to domain formation, while the small plateau around 2 nm V^{-1} between 30 and 40 at.% Ti can be due to the reorganization of domains on the surface of the parent metals. For Ti > 40 at.%, the continuous change of the surface domains combined with the formation of the cubic structure lead to an increase in the oxide formation factors. These changes can be observed in the SEM and XRD plots (Figs. 1 and 2). Oxide formation factor values as high as 2.4 nm V^{-1} were obtained for Ta-65 at.% Ti. At higher Ti concentrations from around Ta-73 at.% Ti on, the oxide formation factors start to be overestimated. This is due to a combined roughness increase and current efficiency decrease generated by the formation of metallic nanocrystals on the surface resembling the structure of the pure Ti thin films (see Fig. 2). The decreased current efficiency can be attributed to side reactions triggered by the surface electronic conduction between the nanocrystals. A dotted line in the

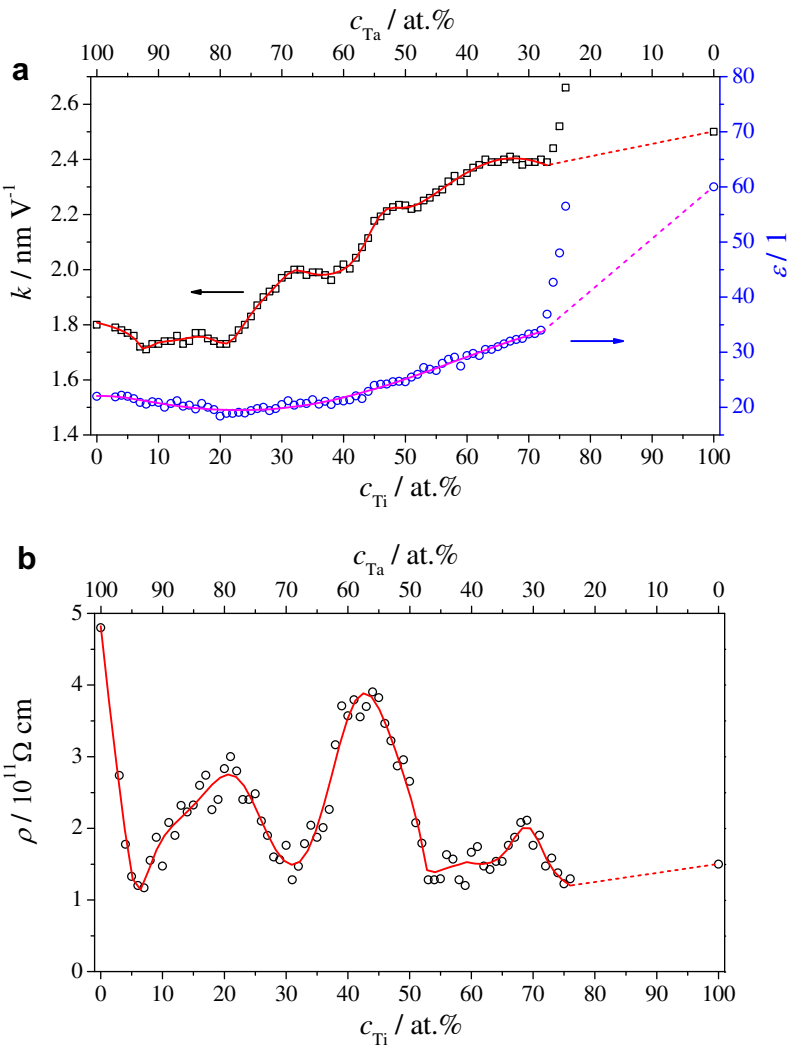

Fig. 5. (a) Oxide formation factors, dielectric constants and (b) electrical resistivities for the anodic oxides grown on the Ta–Ti binary composition spread.

oxide formation mapping (Fig. 5a) is suggesting the trend of a slight further increase up to the value of 2.5 nm V^{-1} for the anodic oxide formation on pure Ti.

The dielectric constant of the anodic oxides grown on the Ta–Ti composition spread shows a smoother behaviour than the oxide formation factor curve. Starting from a value of 22, measured on pure Ta thin films, the dielectric constant initially slightly decreases with the increase of Ti in the alloys. A minimum dielectric constant of around 18 is achieved at Ta-20 at.% Ti. The beginning of the surface grains alignment followed by domain formation with increasing Ti content results in a constant increase of the anodic oxide dielectric constant. An overestimation similar to the one observed in the oxide formation factor curve appears again around Ta-73 at.% Ti. Similar to the extrapolation given before, a dotted line (Fig. 5a) suggests the trend of further dielectric constant increase toward the value of 60 for the anodic oxide on pure Ti.

The electrical resistivity of the anodic oxide mapped in part (b) of Fig. 5 for the entire Ta–Ti composition spread, can also be discussed using the properties of the metal parents shown in Figs. 1 and 2. The relatively high resistivity ($4.8 \times 10^{11}\,\Omega$ cm) of anodic oxide on pure Ta immediately drops by around 50 % upon addition of a few percent of Ti. Several fluctuations are observed in the electrical behaviour of the oxides along the concentration gradient. Here, one should keep in mind the challenge of determining such high impedances when small electrode areas are used. A first peak with a value of around $3 \times 10^{11}\,\Omega$ cm was observed at Ta-20 at.% Ti, coinciding with the threshold for the grain alignment of the parent metal surface. The crystallographic change to the cubic structure at Ta-40 at.% Ti resulted in a sudden increase in the anodic oxide resistivity and a second peak was detected around Ta-45 at.% Ti. A further increase of the Ti concentration led to a lower value of the electrical resistivity ($1.1 \times 10^{11}\,\Omega$ cm) and a small perturbation with an inflexion point around Ta-73 at.% Ti marks the formation of metallic nanocrystals on the surface of the Ta–Ti library. Again here, a dotted line suggests the extrapolation of the electrical resistivity evolution toward the value of pure titania.

3.3. Semiconductor properties by Mott–Schottky analysis

TiO_2 is a semiconductor with a band gap of 3.2 eV, whereas Ta_2O_5 has a 5.1 eV band gap showing insulating properties [23]. Mott–Schottky analysis was applied for investigating the semiconducting properties of the anodic oxides grown on the Ta–Ti composition spread. A thin anodic oxide, locally grown potentiostatically at 3 V, was biased at various potentials without exceeding the maximum oxide formation potential, and the capacitance of the formed space charge layer was determined. The entire surface of the Ta–Ti composition spread was scanned, and in Fig. 6a several curves show the relation between the inverse squared capacitance

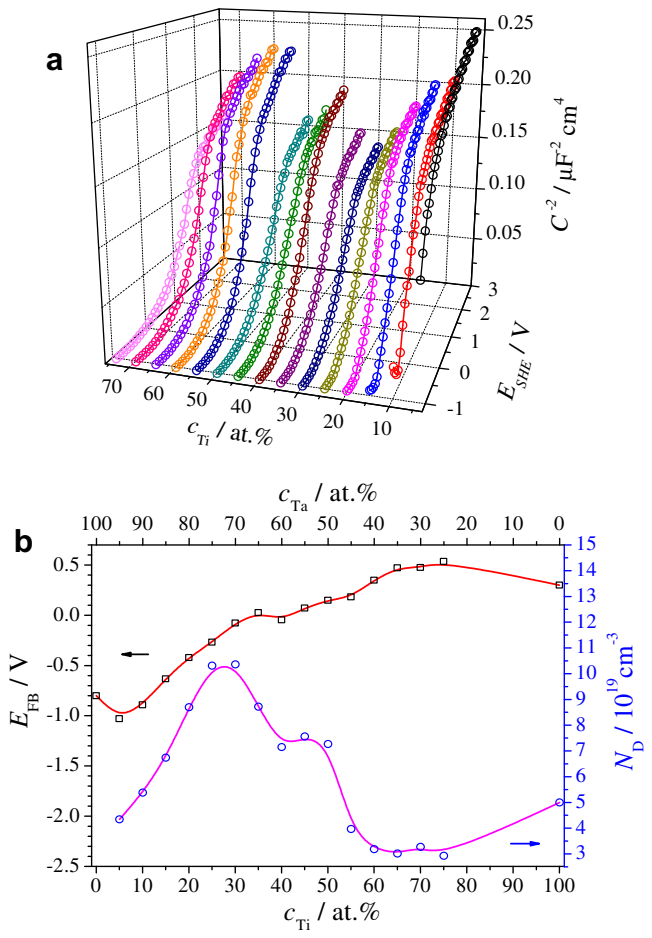

Fig. 6. (a) Mott–Schottky plots and (b) flat band potentials and donor densities for the anodic oxides grown on the Ta–Ti composition spread at different concentrations.

and the applied bias for various concentrations of the parent metals as described by the Mott–Schottky equation:

$$C^{-2} = C_{SC}^{-2} = 2(E - E_{FB} - kT/q_e)/(q_e N_D \varepsilon \varepsilon_0)$$

$E - E_{FB}$ represents the potential difference across the oxide film with E_{FB} being the flat band potential, q_e is the elementary charge of the electron, N_D is the density of the carriers (donors) ε is the dielectric constant (relative permittivity number) of the oxide and ε_0 is the vacuum permittivity. For all Ta–Ti alloys, the presence of an *n* type semiconductor was detected due to the positive slopes of the linear parts of the Mott–Schottky plots from Fig. 6a. The flat band potentials (versus SHE) and the donor concentrations are mapped as a function of parent metal concentrations in part b of Fig. 6. The evolution of the flat band potential of the anodic oxides shows a continuous increase with increasing Ti concentration. Starting from a value of −0.8 V measured on anodic Ta_2O_5 [23], the addition of small amounts of Ti result first in a decrease to around −1 V at Ta-5 at.% Ti. This can be an artefact obtained during the evaluation of the Mott–Schottky curves shown in Fig. 6a due to the fact that a Ti concentration lower than 15 at.% does not clearly present a linear region associated with a semiconducting behaviour. For Ti concentrations >65 at.%, the anodic oxide flat band potential reaches a stable level of around 0.5 V, slightly higher than the value of the pure TiO_2 (0.3 V). The donor concentrations of the anodic oxides grown on the surface of the Ta–Ti combinatorial library show a different dynamic. At low Ti concentrations, the anodic oxides exhibit values around 5×10^{19} cm^{-3} but this value doubles as soon as the threshold for the metallic grain alignment is reached at Ta-25 at.% Ti. With further increasing Ti content, the donor density decreases continuously. A small plateau is seen between 40 and 50 at.% Ti corresponding to the surface domain reorganization of the parent metallic alloy. The surface domains vanishing beyond Ta-60 at.% Ti observed in the SEM images of Fig. 1, is correlated with a constant plateau of the donor density in the anodic oxides at around 3×10^{19} cm^{-3}.

3.4. Surface analytical investigations

XPS depth profiling was used for the analysis of the anodic oxides grown potentiostatically at 10 V. They are presented in Fig. 7 for several concentrations of the Ta–Ti composition spread. The values of the binding energies corresponding to the metals or oxides are indicated in each graph and the depth scale calibrated using SiO_2 is given on the right side of the spectra. All peaks, corresponding to both metal and anodic oxide, progressively change their intensity with the increase of Ar sputtering time. The positions of the 4f peaks corresponding to Ta suggest the presence of Ta_2O_5 on the surface of the Ta–Ti composition spread, independent on the parent metal concentration. The same trend was observed for the Ti peaks together with a small initial shift (down to 2 nm in-depth) due to surface charge accumulation during the measurements. At depths larger than 2 nm on the SiO_2 scale, the measured binding energies of the 2p and 4f peaks confirm the presence of TiO_2 together with Ta_2O_5, suggesting a mixed oxide growth. Following the depth profiles, the positions of the oxide peaks slightly shift toward lower energies when approaching the oxide/metal interface. This shift is more obvious for Ta and is due to a local oxide reduction during the sputtering process. In all the investigated anodic oxides, metallic species could be detected together with the oxides starting at a depth of around 20 nm for Ti and 4–6 nm for Ta. These metallic atoms represent ions trapped in the anodic oxide during the potentiodynamic anodization, which were reduced due to Ar sputtering. The amplitudes of the TiO_2 peaks close to the surface of the mixed oxide increase with the increase of Ti concentration, while the Ta_2O_5 peaks have a more constant behaviour. The XPS spectra measured on the surface of the anodic oxides (before sputtering) were quantitatively evaluated by integrating the 2p and 4f doublets for TiO_2 and Ta_2O_5, respectively. The required sensitivity factors were taken from MultiPack© software [24]. The C and O peaks were also included in the total evaluation, and the relative concentration of the oxides was recalculated for determining their ratio. The integration of the spectra recorded on the surface of the oxides shows that the ratio between the TiO_2 and Ta_2O_5 concentrations in the mixed anodic oxide is generally larger than the Ti/Ta ratio in the metallic parent alloys. This can be attributed to a higher transport number of Ti (0.35) as compared with Ta (0.24) [25,26]. Table 1 summarizes the values of the oxide concentrations measured at several positions in the Ta–Ti combinatorial library together with their deviations as compared to the metal parent alloy. The amount of Ta in the anodic oxides falls behind that of the parent metal by about 14% for concentrations of Ti of up to 35 at.%, before the formation of domains was observed in the SEM images (Fig. 1). The anodic oxides grown in the concentration range at the end of the domain reorganization region and the zone of nanocrystal formation, show similar behaviours, Ta concentration being 34% smaller than the Ta concentration in the parent alloys. The concentration of Ti in the mixed anodic oxides followed a different trend, starting with an increase of 78% for Ta-15 at.% Ti. The compositional range for the domain reorganization, found between Ta-35 and Ta-55 at.% Ti show a Ti enrichment by approximately 27% in the anodic oxides, whereas an increase by 12% was seen in the nanocrystal formation region. This analysis shows the relevance of the structural changes in the parent metal alloys, which are reflected in the properties of the anodic oxides and their growth behaviour.

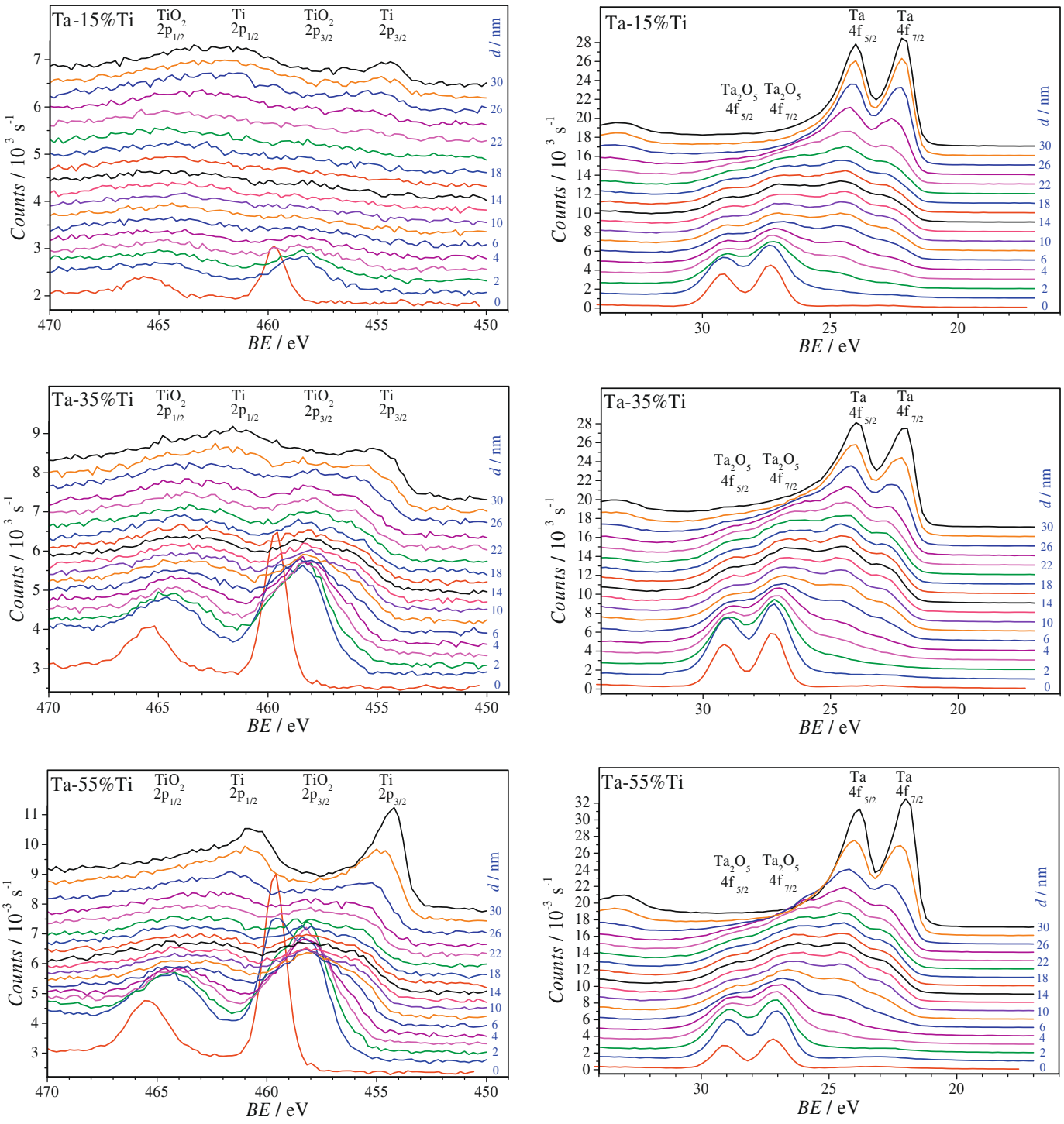

Fig. 7. XPS depth profiling spectra of the anodic oxides potentiodynamically grown at 10 V on the Ta–Ti composition spread at different compositions.

Table 1
The metal concentration ratios for the parent metal alloys (Me), anodic oxides (Ox) and their individual variations with respect to the metal concentrations ($\Delta^{Me;Ox}$).

Ta_{Me}:Ti_{Me} (at.%)	Ta_{Ox}:Ti_{Ox} (at.%)	$\Delta^{Me;Ox}$ Ta (%)	$\Delta^{Me;Ox}$ Ti (%)
85:15	73.3:26.7	−13.8	+78
65:35	55.4:44.6	−14.8	+27.4
45:55	29.7:70.3	−34	+27.8
25:75	15.9:84.1	−36.4	+12.1

4. Conclusions

The concept of investigating the passivation kinetics in the Ta–Ti system by means of high-throughput scanning on a composition spread sample prepared by co-sputtering of the metals was successfully applied. It allowed study of the anodisation process, revealing that all oxide films formed on the various alloys showed good passivation behaviour without notable side reactions such as oxygen evolution. Composition dependent changes in the film for-

mation factor and relative permittivity number were measured, delivering a complete data set in this binary library.

For the structure of the parent metal alloy, three distinct regions were identified: small compact grains, a transitional alignment zone followed by the formation of domains, their reorganization, and then nanocrystal formation.

Ta-rich regions were found to have tetragonal symmetry at low Ti concentrations, and the parent alloys are stabilized in a cubic symmetry for Ti contents >40 at.%.

Significant changes in the electrochemical properties as a function of the alloy composition were found, which in each case could be directly correlated to the nanoscopic change of the morphology in the structure of the base alloy, e.g. phase change.

The composition of the anodic oxides with respect to the metal concentration ratio is slightly different from the composition of the underlying parent metal alloys. This is attributed to the different transport numbers of Ta and Ti which was observed earlier for thicker oxides on alloys of fixed composition, and is therefore in good agreement with the data reported there.

This work presents a novel approach in studying the passivation of binary alloys, as it yields results on the entire range of compositions. Further studies will focus on the various deposition methods, since they should allow intentional changes of the alloy morphology and thus the influence of factors such as chemical composition, phase and crystallographic orientation.

Acknowledgement

A.I. Mardare acknowledges IMPRS SurMat for financial support through a fellowship caesar Institute in Bonn is acknowledged for the co-depositions of the Ta–Ti thin films.

References

[1] W. Gregor, Chemische Annalen für die Freunde der Naturlehre, Arzneygelahrtheit, Haushaltungskunst und Manufacturen, 1791.
[2] J.W. Schultze, A.W. Hassel, Encyclopedia of Electrochemistry, Wiley-VCH, Weinheim, 2003.
[3] M. Hansen, Constitution of Binary Alloys: Metallurgy and Metallurgical Series, second ed., McGraw-Hill Book Company, New York, Toronto, London, 1958.
[4] Y.L. Zhou, M. Niinomi, T. Akahori, Effects of Ta content on Young's modulus and tensile properties of binary Ti–Ta alloys for biomedical applications, Mater. Sci. Eng. A 371 (2004) 283.
[5] Y.G. Chen, B.X. Liu, Metastable alloys synthesized by ion mixing in immiscible Ti–Nb and Ti–Ta systems, Mater. Sci. Eng. B52 (1998) 1.
[6] R.L. Ruth, N. Schwartz, A Rutherford Backscattering Analysis of Anodic Tantalum-Titanium Oxides, J. Electrochem. Soc. 123 (1976) 1860.
[7] R.J. Hanrahan Jr., D.P. Butt, Oxidation Kinetics and Mechanisms of Ti–Ta alloys, Oxidation Metals 47 (1997) 317.
[8] A.W. Hassel, L. Neelakantan, A. Zelenkevych, A. Ruh, M. Spiegel, Selective de-alloying of NiTi by oxochloridation, Corr. Sci. 50 (2008) 1368.
[9] K. Alves de Souza, A. Robin, Preparation and characterization of Ti–Ta alloys for application in corrosive media, Mater. Lett. 57 (2003) 3010.
[10] Y.L. Zhou, M. Niinomi, H. Fukui, T. Akahori, H. Toda, Effects of Ta content on Young's modulus and tensile properties of binary Ti–Ta alloys for biomedical applications, Mater. Sci. Eng. A398 (2005) 28.
[11] S. Mato, G. Alcala, P. Skeldon, G.E. Thompson, A.B. Mann, D. Masheder, H. Habazaki, K. Shimizu, Dielectric and mechanical properties of anodic films in the Ta–Ti system, Surf. Interf. Anal. 35 (2003) 477.
[12] A.I. Mardare, A.P. Yadav, A.D. Wieck, M. Stratmann, A.W. Hassel, Combinatorial electrochemistry on Al–Fe alloys, Sci. Technol. Adv. Mater. 9 (2008) 035009.
[13] A.W. Hassel, M.M. Lohrengel, The scanning droplet cell and its application to structured nanometer oxide films on aluminium, Electrochim. Acta 42 (1997) 3327.
[14] A.I. Mardare, A.D. Wieck, A.W. Hassel, Microelectrochemical lithography: A method for direct writing of surface oxides, Electrochim. Acta 52 (2007) 7865.
[15] K.A. Lill, A.W. Hassel, A combined μ-mercury reference electrode/Au counter-electrode system for microelectrochemical applications, J. Solid State Electrochem. 10 (2006) 941.
[16] M.M. Lohrengel, A. Moehring, M. Pilaski, Capillary-based droplet cells: limits and new aspects, Electrochim. Acta 47 (2001) 137.
[17] A.I. Mardare, A.W. Hassel, "Quantitative optical recognition of highly reproducible ultra thin oxide films in microelectrochemical anodisation", Rev. Sci. Instr., submitted for publication.
[18] J.L. Murray, Binary alloy phase diagrams. ASM International, 1990.
[19] J. Kunze, A. Ghicov, H. Hildebrand, J.M. Macak, L. Traviera, P. Schmuki, Challenges in the surface analytical characterisation of anodic TiO_2 films – a review, Z. Phys. Chem. 219 (2005) 1561.
[20] J.F. McAleer, L.M. Peter, Photocurrent Spectroscopy of Anodic Oxide Films on Titanium, Faraday Discuss. 70 (1980) 67.
[21] A.W. Hassel, D. Diesing, Breakdown of ultrathin anodic valve metal oxide films in metal-insulator-metal-contacts compared with metal-insulator-electrolyte contacts, Thin Solid Films 414 (2002) 296.
[22] M.M. Lohrengel, Thin anodic oxide layers on aluminium and other valve metals: high field regime, Mater. Sci. Eng. R11 (1993) 243.
[23] J.W. Schultze, M.M. Lohrengel, Stability, reactivity and breakdown of passive films. Problems of recent and future research, Electrochim. Acta 45 (2000) 2499.
[24] MultiPack software manual version 6.0, Physical Electronics.
[25] H. Habazaki, K. Shimizu, S. Nagata, P. Skeldon, G.E. Thompson, G.C. Wood, Ionic Mobilities in Amorphous Anodic Titania, J. Electrochem. Soc. 149 (2002) B70.
[26] J.P.S. Pringle, Transport Numbers of Metal and Oxygen during the Anodic Oxidation of Tantalum, J. Electrochem. Soc. 120 (1973) 398.